J Physiol 595.7 (2017) pp 2253–2268

The Journal of Physiology

Quantitative analysis of the Ca^{2+}-dependent regulation of delayed rectifier K^+ current I_{Ks} in rabbit ventricular myocytes

Daniel C. Bartos, Stefano Morotti, Kenneth S. Ginsburg, Eleonora Grandi and Donald M. Bers

Department of Pharmacology, University of California, Davis, Davis, CA 95616, USA

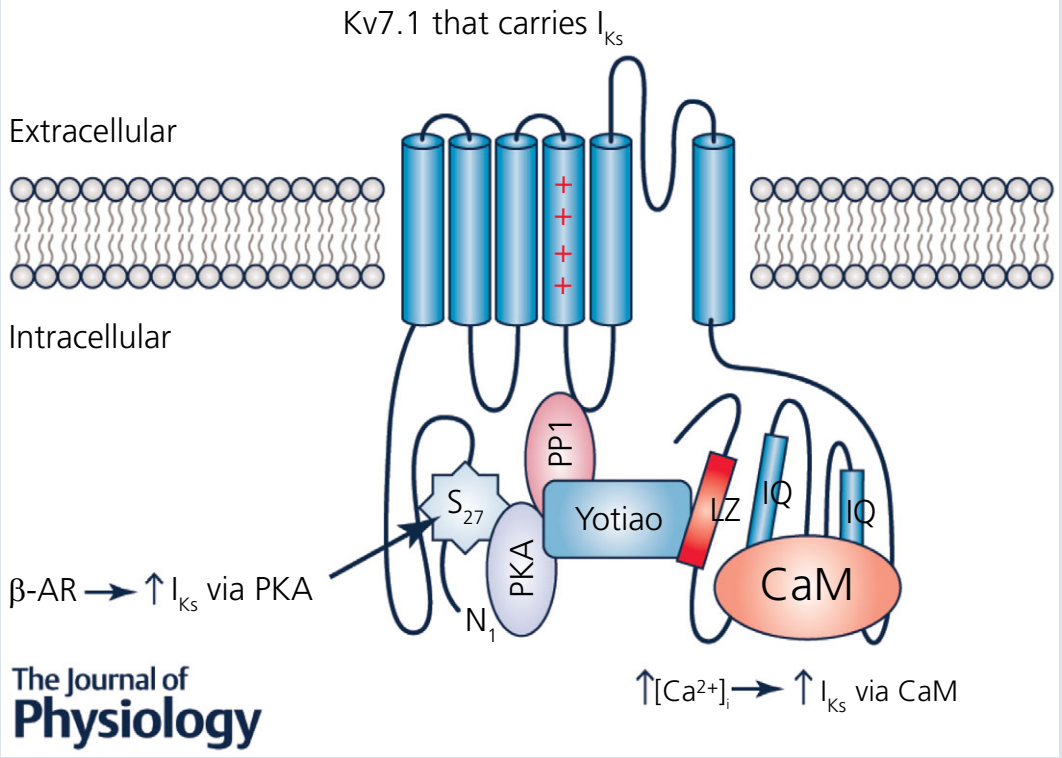

Abstract The slowly activating delayed rectifier K^+ current (I_{Ks}) contributes to repolarization of the cardiac action potential (AP). Intracellular Ca^{2+} ($[Ca^{2+}]_i$) and β-adrenergic receptor (β-AR) stimulation modulate I_{Ks} amplitude and kinetics, but details of these important I_{Ks} regulators and their interaction are limited. We assessed the $[Ca^{2+}]_i$ dependence of I_{Ks} in steady-state conditions and with dynamically changing membrane potential and $[Ca^{2+}]_i$ during an AP. I_{Ks} was recorded from freshly isolated rabbit ventricular myocytes using whole-cell patch clamp. With intracellular pipette solutions that controlled free $[Ca^{2+}]_i$, we found that raising $[Ca^{2+}]_i$ from 100 to 600 nM produced similar increases in I_{Ks} as did β-AR activation, and the effects appeared additive. Both β-AR activation and high $[Ca^{2+}]_i$ increased maximally activated tail I_{Ks}, negatively shifted the voltage dependence of activation, and slowed deactivation kinetics. These data informed changes in our well-established mathematical model of the rabbit myocyte. In both AP-clamp experiments and simulations, I_{Ks} recorded during a normal physiological Ca^{2+} transient was similar to I_{Ks} measured with $[Ca^{2+}]_i$ clamped at 500–600 nM. Thus, our study provides novel quantitative data as to how physiological $[Ca^{2+}]_i$ regulates I_{Ks} amplitude and kinetics during the normal rabbit AP. Our results suggest that micromolar $[Ca^{2+}]_i$, in the submembrane or junctional cleft space, is not required to maximize $[Ca^{2+}]_i$-dependent I_{Ks} activation during normal Ca^{2+} transients.

DOI: 10.1113/JP273676

Key points

- $[Ca^{2+}]_i$ enhanced rabbit ventricular slowly activating delayed rectifier K^+ current (I_{Ks}) by negatively shifting the voltage dependence of activation and slowing deactivation, similar to perfusion of isoproterenol.
- Rabbit ventricular rapidly activating delayed rectifier K^+ current (I_{Kr}) amplitude and voltage dependence were unaffected by high $[Ca^{2+}]_i$.
- When measuring or simulating I_{Ks} during an action potential, I_{Ks} was not different during a physiological Ca^{2+} transient or when $[Ca^{2+}]_i$ was buffered to 500 nM.

(Resubmitted 16 November 2016; accepted after revision 12 December 2016; first published online 23 December 2016)
Corresponding author D. M. Bers: Department of Pharmacology, University of California, Davis, Genome Building Rm 3503, 451 Health Sciences Drive, Davis, CA 95616, USA. Email: dmbers@ucdavis.edu

Abstract figure legend Membrane topology of a Kv7.1 α-subunit and regulatory proteins.

Abbreviations AP, action potential; β-AR, β-adrenergic receptor; CaM, calmodulin; $[Ca^{2+}]_i$, intracellular calcium; CaT, Ca^{2+} transient; k, slope-factor for the V_m dependence of activation; I_{CaL}, L-type Ca^{2+} current; I_{CFTR}, cystic fibrosis transmembrane conductance regulator Cl^- current; $I_{Cl,Ca}$, Ca^{2+}-activated Cl^- current; I_{Ks}, slowly activating delayed rectifier K^+ current; I_{Kr}, rapidly activating delayed rectifier K^+ current; ISO, isoproterenol; I_{MAX}, maximally activated current; I–V, current–voltage; PKA, protein kinase A; PKC, protein kinase C; PLM, phospholemman; τ_{act}, time course of activation; τ_{deact}, time course of deactivation; $V_{1/2}$, half-maximal activation potential; V_m, membrane potential.

Introduction

In the heart, the repolarizing delayed rectifier potassium current (I_K) consists of a slowly activating component (I_{Ks}) and a rapidly activating component (I_{Kr}) that differ in drug sensitivity, and voltage- or time-dependent properties (Sanguinetti & Jurkiewicz, 1990; Selnick *et al.* 1997). These outward currents are required during phase 2 and phase 3 of the ventricular action potential (AP) for cardiac repolarization (Nerbonne & Kass, 2005). Under normal physiological conditions and in the absence of β-adrenergic stimulation, I_{Kr} plays a primary role in repolarization in large mammals (such as rabbit, dog and human). I_{Ks} density has typically been measured to be much lower than I_{Kr} in these animals under basal conditions, but these studies were performed in situations where intracellular Ca^{2+} ($[Ca^{2+}]_i$) was highly buffered (Jost *et al.* 2007). Additionally, most studies of I_{Ks} in native systems are performed in guinea pig, where I_{Ks} density is very large, and activation and deactivation kinetics are significantly slower than human I_{Ks}. Rabbit and dog I_{Ks} more closely resemble human I_{Ks}, thus making these species more suitable to use when studying I_{Ks} function and regulation (Liu & Antzelevitch, 1995; Heath & Terrar, 1996; Li *et al.* 1996; Salata *et al.* 1996). Furthermore, because repolarization depends on a fine balance between inward (mainly Ca^{2+}-selective) and outward (K^+-selective) currents, I_{Ks} might play an important role when normal repolarization reserve is impaired (Jost *et al.* 2005; Grandi *et al.* 2010).

The I_{Ks} macromolecular channel complex minimally consists of the Kv7.1 pore-forming α-subunit and the ancillary MinK1 β-subunit (Barhanin *et al.* 1996; Sanguinetti *et al.* 1996). 'Loss-of-function' mutations within the genes encoding Kv7.1 (*KCNQ1*) or MinK1 (*KCNE1*) typically cause a decrease in I_{Ks} and are linked to congenital arrhythmia syndromes, type 1 and type 5 long QT syndromes (LQT1 and LQT5), respectively (Wang *et al.* 1996; Splawski *et al.* 1997). The dysfunctional I_{Ks} may lead to prolongation of the QT interval on a patient's electrocardiogram (ECG) and increases the risk for the phenotypic polymorphic ventricular tachycardia, torsades de pointes (El-Sherif *et al.* 1997; Shah *et al.* 2005). Interestingly, the onset of torsades de pointes in LQT1 patients is typically triggered by adrenergic stress, highlighting the physiological importance of β-adrenergic regulation in mediating the cardiac AP and specifically I_{Ks} (Schwartz *et al.* 2001; Goldenberg *et al.* 2012). During β-adrenergic stimulation, Kv7.1 is phosphorylated by protein kinase A (PKA) on the amino terminus and causes an increase of I_{Ks} that is important for normal AP shortening (Walsh & Kass, 1988; Marx *et al.* 2002). Mutations that disrupt the β-adrenergic upregulation of I_{Ks} are also linked to LQT1, further emphasizing the importance of this process (Heijman *et al.* 2012; Bartos *et al.* 2014). Interestingly, $[Ca^{2+}]_i$ can also influence I_K (sum of I_{Kr} and I_{Ks}), and β-adrenergic stimulation increases Ca^{2+} transients (CaTs) in myocytes (Tohse, 1990; Bers, 2002). Dynamic clamp experiments in guinea pig myocytes demonstrated that I_{Ks} was larger than I_{Kr} subsequent to β-adrenergic stimulation (Banyasz *et al.* 2014). This is an important finding because these recordings are in conditions where $[Ca^{2+}]_i$ is not buffered and physiological membrane and Ca^{2+} dynamics are maintained (Banyasz *et al.* 2011).

Several studies have reported on the regulation of I_K by $[Ca^{2+}]_i$ by using the whole-cell and inside-out patch clamp methods. The results suggested that increasing $[Ca^{2+}]_i$ (similar to the rise in $[Ca^{2+}]_i$ during each cycle of contraction and relaxation from ∼0.1 to 1 μM) in guinea pig ventricular myocytes increases I_K, most likely by increasing the open probability (P_O) or number of channels at the cell surface (Tohse, 1990). A later study determined calmodulin (CaM) is required for Ca^{2+}-sensitive increases of I_K, and this process was PKA and protein kinase C (PKC) independent (Nitta *et al.* 1994). Because Ca^{2+}–CaM interaction with nitric oxide synthase (NOS) is an important determinant for NOS activation and NO release (Bai *et al.* 2004, 2005), the same group also showed that NO enhancement of I_{Ks} is critical for regulating AP duration, Ca^{2+} sensitivity of I_{Ks} itself, and intracellular Ca^{2+} cycling (Bai *et al.* 2005). More recently, two studies reported that CaM binds to IQ motifs on the C-terminus of Kv7.1, and CaM interaction with the I_{Ks} channel complex is required for proper channel assembly, Ca^{2+} sensitivity and cell surface expression (Ghosh *et al.* 2006; Shamgar *et al.* 2006). Additionally, LQT1-linked mutations can disrupt the CaM–Kv7.1 interaction, uncover inactivation of I_{Ks} and decrease I_{Ks} similar to other defined loss-of-function mutations (Ghosh *et al.* 2006; Shamgar *et al.* 2006).

While previous studies have suggested the importance of $[Ca^{2+}]_i$ regulation of I_{Ks}, quantitative information as to how Ca^{2+} sensitivity of I_{Ks} may affect cardiac repolarization in a more physiologically relevant environment is lacking. We sought to fill this gap in knowledge here.

Methods

Ethical approval

All animal care and procedures were approved by the University of California, Davis Institutional Animal Care and Use Committee and are in accordance with National Institutes of Health guidelines.

Rabbit euthanasia and ventricular myocyte isolation

Adult male New Zealand White rabbits (source, Western Oregon Rabbit Company) were housed at the University of California, Davis vivarium with access to normal food and water *ad libitum*. Rabbit ventricular myocytes were isolated with techniques modified from Pogwizd *et al.* (1999, 2001) and used acutely. Rabbits were administered Heparin, at 400 units kg^{-1} subcutaneously, 15–30 min before surgery. Animals were then placed in a conventional restraint cage and given propofol at 0.5–2 mg kg^{-1} or to effect. Once sedated, rabbits were gently but quickly removed from the restrainer and masked for isoflurane inhalation while being placed supine for surgery. Isoflurane was delivered with 100% oxygen through a facemask via a regularly calibrated veterinary vaporizer at a flow rate of 3–4 l min^{-1}, initially at 3–4.5% but reduced as appropriate as long as full areflexia was assured. Once very deep anaesthesia was verified, the heart was rapidly excised. Therefore, the animals only experienced brief restraint and minor discomfort of the injection.

Excised hearts were quickly washed in Ca^{2+}-free normal Tyrode solution at 4°C. They were then cannulated via the aorta for retrograde Langendorff perfusion. Oxygenated Hepes-buffered Ca^{2+}-free Tyrode solution at 37°C was perfused long enough to ensure clearing of blood and Ca^{2+}, resulting in arrest and relaxation. Pressure was ∼60–80 mmHg and flow rate was ∼20–30 ml min^{-1}. Perfusion was then switched to the same Tyrode solution containing either a crude collagenase (∼1 mg ml^{-1}) and protease (∼0.05 mg ml^{-1}) mixture or a defined enzyme product such as Roche Liberase (collagenase/thermolysin) at an equivalent concentration, with $[Ca^{2+}]$ adjusted to 20–25 μM. The tissue softened within 20–30 min, at which time the heart was removed and minced into 1–2 mm pieces in Tyrode solution containing 1% BSA. The pieces were gently agitated or triturated and passed through a nylon mesh of 200–250 μm pitch, resulting in liberation of individual cells, which were washed free of BSA and maintained at room temperature in Tyrode solution containing 50 μM Ca^{2+} until the time of the experiments.

Electrophysiology

Cardiac myocytes were plated on laminin-coated glass coverslips at room temperature and transferred to an inverted microscope (Leica DMI3000B; Leica Microsystems; Buffalo Grove, IL, USA). Patch pipettes were fabricated from thin-walled, filamented borosilicate glass and fire polished (World Precision Instruments; Sarasota, FL, USA). Uncompensated pipette resistances were ∼1–1.8 MΩ. Only cells with seal resistances > 1 GΩ were used for recordings and series resistance was compensated up to 80%. pCLAMP 10.4 (Molecular Devices; Sunnyvale, CA, USA) was used to generate the voltage clamp protocols, acquire current signals, and initiate data analyses. An Axopatch-200A patch clamp amplifier (Axon Instruments/Molecular Devices) was used to measure membrane current and cell capacitance. The giga seal was obtained in normal Tyrode solution containing (in mM): 135 NaCl, 0.33 NaH_2PO_4, 5.4 KCl, 2 $CaCl_2$, 0.53 $MgCl_2$, 5.5 glucose and 5 Hepes (pH adjusted to 7.4 with NaOH). Once the cell membrane was ruptured and the whole-cell configuration was obtained, the external solution was switched to and continuously superfused at room temperature for experiments using square pulses as the voltage (V_m) command, or at 37°C for experiments implementing an AP waveform as the

V_m command, with the I_{Ks} recording solution containing (in mM): 132 NaCl, 4 KCl, 1.8 $CaCl_2$, 1.2 $MgCl_2$, 0.2 $BaCl_2$, 10 glucose, 10 Hepes, 5 4-aminopyridine (4-AP), 0.01 nifedipine, and 0.003 dofetilide (pH adjusted to 7.4 with NaOH). 4-AP, nifedipine, and dofetilide were obtained from Sigma-Aldrich (St Louis, MO, USA). For I_{Kr} recordings, dofetilide was replaced with the I_{Ks}-selective inhibitor HMR-1556 (0.001 mM, Tocris Bioscience; Bristol, UK) to block I_{Ks}. To obtain $[Ca^{2+}]_i$ signals, Fluo-4 K^+-salt (0.05 mM) was included in the intracellular pipette solution (described below). For most experiments $[Ca^{2+}]_i$ was buffered using a combination of 5 mM BAPTA (K_d ~190 nM) plus 1 mM dibromo-BAPTA 4K (K_d ~1.8 μM) in the pipette solution. Total $[Ca^{2+}]_i$ was adjusted to achieve free $[Ca^{2+}]_i$ of 0, 100, 300, 500 and 600 nM, using the MaxChelator program (http://www.stanford.edu/~cpatton/maxc.html). In some experiments we let the myocyte control free $[Ca^{2+}]_i$, in which case millimolar BAPTA + dibromo-BAPTA were replaced with 0.05 mM EGTA. In addition, the intracellular pipette solution contained (in mM): 120 KOH, 20 KCl, 2 $MgCl_2$, 5 Mg-ATP, 10 Hepes, 0.003 CaM and 100 aspartic acid (pH adjusted to 7.2 with KOH). I_{Ks} was recorded initially within 2–4 min once the Ca^{2+}-signal and I_{Ks} amplitude reached steady-state. Depolarizing square-pulses every 15 s allowed monitoring of both I_{Ks} and Ca^{2+} signals. For experiments involving β-adrenergic stimulation, 50 nM isoproterenol (ISO) was perfused in the extracellular solution after an initial current-voltage (*I-V*) protocol was recorded, and after 5 min an additional *I–V* was measured.

For measuring I_{Ks} during an AP waveform, a rabbit ventricular AP waveform previously recorded at 1 Hz was implemented as the V_m command, also at 1 Hz. No drugs were used for initial recordings. The first 50 sweeps were averaged as the control current activated during the AP waveform. Then, 1 μM HMR-1556 was added to the extracellular solution, and 50 more sweeps were recorded and averaged, then subtracted in order to define the HMR-sensitive I_{Ks}. All AP-clamp current recordings were performed at 35–37°C using an in-line and bath temperature control system (Warner Instruments; Hamden, CT, USA).

Standard epifluorescence microscopy

Changes in $[Ca^{2+}]_i$ were monitored using wide-field epifluorescence microscopy. The intracellular pipette solution was modified to contain 0.05 mM Fluo-4 pentapotassium salt (Thermo Fisher Scientific; New York, NY, USA) for experiments using the whole-cell patch clamp technique. Cells were preloaded with cell permeable Fluo-4 AM (Thermo Fisher Scientific) for 28 min in a Ca^{2+}-free Tyrode solution containing 10 μM Fluo-4 AM (K_d for Ca^{2+} of ~335 nM). Fluo-4 was excited by light of 488 nm wavelength, and emission was detected using a 514 nm long-pass filter. The wavelength of excitation was controlled by an Optoscan monochromator (Cairn Research; Faversham, UK), and the emission signal was detected by a photomultiplier tube.

Mathematical modelling and simulation

We modified the Hodgkin–Huxley type formulation of I_{Ks} in our rabbit ventricular model (Shannon *et al.* 2004; Negroni *et al.* 2015) to fit the experimentally observed Ca^{2+}- and ISO-dependent regulation of maximal current, activation $V_{1/2}$, and deactivation kinetics. Experimental data were scaled to 37°C using a Q_{10} of 2.5 for both maximal conductance and time constants of activation and deactivation.

I_{Ks} channels are assumed to be uniformly distributed on the sarcolemma. This means that 11% are in junctional clefts with the SR ($I_{Ks\text{-junc}}$ *vs.* 89% in the external sarcolemma, $I_{Ks\text{-sl}}$), corresponding with the fraction of rabbit ventricular myocyte sarcolemma involved in such junctions (21% of T-tubular membrane plus 4.6% of surface sarcolemma; Shannon *et al.* 2004). This accounts for local differences in $[Ca^{2+}]_i$ that occur at the cleft and subsarcolemmal space. Total current is defined by the following equation:

$$I_{Ks} = I_{Ks-junc} + I_{Ks-sl}$$

Each component is calculated using the following formulation:

$$I_{Ks-c} = F_{Ks-c}\, G_{Ks-c}\, x_s^2\, (E_m - E_{Ks-c})$$

$$E_{Ks-c} = \frac{RT}{F} \ln \frac{[K]_o + p_{NaK}[Na]_o}{[K]_c + p_{NaK}[Na]_c}$$

$$\frac{dx_s}{dt} = \frac{x_{s,\infty} - x_s}{\tau_{xs}}$$

$$x_{s,\infty} = 1/\left(1 + e^{-(E_m - V_{1/2})/25}\right)$$

$$\tau_{xs} = 100 + \frac{100 + 700e^{-\frac{(E_m+30)^2}{4000}}}{1 + e^{-\frac{(E_m + V_{\tau 1/2})}{10}}}$$

where c represents either the junctional ($F_{Ks\text{-junc}} = 0.11$) or subsarcolemmal ($F_{Ks\text{-sl}} = 0.89$) compartment, and the Na^+:K^+ permeability ratio (p_{NaK}) of the channel is 0.01833. Note that each compartment senses different Ca^{2+} and Na^+ concentrations ($[Ca]_c$ and $[Na]_c$ in this formulation). However, as opposed to Ca^{2+}, significant $[Na^+]$ gradients are not seen in the model during excitation contraction coupling.

PKA- and Ca^{2+}-dependent modulation of I_{Ks} is modelled as follows:

$$G_{Ks-c} = G_{Ks0} + \frac{\Delta G_{Ks}}{1 + (150e^{-6}/[Ca]_c)^{1.3}}$$

$$V_{1/2-c} = V_{h0} + \frac{\Delta V_h}{1 + (350e^{-6}/[Ca]_c)^4}$$

$$V_{\tau 1/2-c} = V_{\tau 0} + \frac{\Delta V_\tau}{1 + (150e^{-6}/[Ca]_c)^3}$$

$$G_{Ks0} = 0.010 + 0.010\ k_{PKA}[mS\mu F^{-1}]$$

$$\Delta G_{Ks} = 0.030 + 0.015\ k_{PKA}[mS\mu F^{-1}]$$

$$V_{h0} = -1 - 10\ k_{PKA}\ [mV]$$

$$\Delta V_h = -11 + 1\ k_{PKA}$$

$$V_{\tau 0} = 26 + 9\ k_{PKA}\ [mV]$$

$$\Delta V_\tau = 14 - 5\ k_{PKA}\ [mV]$$

where the parameters G_{Ks0}, ΔG_{Ks0}, V_{h0}, ΔV_h, $V_{\tau 0}$ and ΔV_τ are fitted to the experimentally observed changes in G_{Ks}, $V_{1/2}$, and $V_{\tau 1/2}$ with ISO. These parameters are modulated by the scale factor, k_{PKA} (varying between 0 and 1) given by:

$$k_{PKA} = \frac{PKA_p - 0.1098}{0.7282}$$

where PKA_p is the fraction of I_{Ks} phosphorylated by PKA (I_{Ksp}) over total I_{Ks} (I_{Kstot}), calculated as in (Negroni *et al.* 2015):

$$PKA_p = \frac{I_{Ksp}}{I_{Kstot}}$$

and 0.1098 is basal PKA_p (in the absence of ISO) and 0.7282 is the difference between PKA_p at ISO = 100 nM (corresponding to 'maximal activation') and basal PKA_p.

AP and current-clamp simulations were performed incorporating the new I_{Ks} model within our well-established rabbit ventricular model (as last updated in Negroni *et al.* 2015). The same AP waveform used for experiments was given as a V_m command in AP-clamp simulations (1 Hz). APs were simulated at 3 Hz in the absence or presence of 20 and 50 nM [ISO]. In addition to I_{Ks}, PKA targets were: L-type Ca^{2+} current (I_{CaL}), ryanodine receptor, phospholamban, phospholemman (PLM), I_{Kr}, cystic fibrosis transmembrane conductance regulator Cl^- current (I_{CFTR}), Ca^{2+}-activated Cl^- current ($I_{Cl,Ca}$), troponin I, titin and myosin binding protein C. Model differential equations were implemented in Matlab (The Mathworks Inc., Natick, MA, USA) and solved numerically using a variable order solver (ode15s). The code is available for download at: https://somapp.ucdmc.ucdavis.edu/Pharmacology/bers/

Analysis and statistics

I–V relations were plotted for the peak I_{Ks} (normalized to capacitance, pA pF^{-1}) measured at the end of the step pulse or at the initiation of the tail pulse. Origin 7.0 (OriginLab Corp.; Northhampton, MA, USA) was used for performing Boltzmann fitting and plotting *I–V* graphs. The following Boltzmann equation was used to describe the *I–V* relations:

$$I = I_{MIN} + (I_{MAX} - I_{MIN})/(1 + e^{(V_{1/2} - V)/k})$$

where I_{MIN} is the minimally activated I_{Ks}, I_{MAX} is the maximally activated I_{Ks} (pA pF^{-1}), $V_{1/2}$ is the midpoint potential for half-maximal activation of I_{Ks} (mV), and k is the slope factor (mV per e-fold change). The time course of activation and deactivation (τ_{act} and τ_{deact}, respectively) were determined by fitting a single exponential equation using pCLAMP 10.4 software. Data were reported as the mean ± standard error of the mean (SEM). Student's paired or unpaired *t* test was performed when appropriate to determine if values were different from one another. For comparison of three or more groups, a one-way ANOVA was performed with Tukey's *post hoc* analysis. Significance was determined when $P < 0.05$.

Results

Distinguishing the delayed rectifier K^+ currents, I_{Ks} and I_{Kr}

Figure 1 shows control experiments to demonstrate how we distinguished between rabbit I_{Ks} and I_{Kr}. To isolate total I_K (sum of I_{Ks} and I_{Kr}), we blocked I_{K1}, I_{to} and I_{CaL} by using Ba^{2+}, 4-AP and nifedipine, respectively (Fig. 1*A*; with *I–V* protocol in inset). Figure 1*A* shows total delayed rectifier I_K (i.e. $I_{Kr} + I_{Ks}$) with the expected slow I_{Ks} activation during depolarized V_m and the large tail current upon repolarization as expected for I_{Kr}. When recording I_{Kr}, HMR-1556 was added to block I_{Ks} (Fig. 1*B*; note the typical I_{Kr} tail currents that exceed I_{Kr} during the 'step' pulse). To isolate I_{Ks}, we used 3 μM dofetilide (instead of HMR) to block I_{Kr} (Fig. 1*C*). The remaining time-dependent currents were then completely abolished by 1 μM of the I_{Ks} selective inhibitor HMR-1556 (Fig. 1*D*), leaving only a small linear leak current.

Preliminary experiments showed that blockade of $I_{Cl,Ca}$ using 30 μM niflumic acid did not alter I_{Ks} when $[Ca^{2+}]_i$ was low or high, so niflumic acid was not included in the extracellular bath. I_{Ks} currents are small and subject to rundown, and an exemplar time course of our protocol before and after perfusion of ISO (with high pipette $[Ca^{2+}]$) is shown in Fig. 1*E*. There was typically some initial rundown immediately after membrane rupture (and we monitored I_{Ks} single square pulses every 15 s). I_{Ks} usually stabilized within 2–4 min, at which time we performed a full *I–V* set. ISO was added immediately after the *I–V* protocol. Once I_{Ks} stabilized with ISO (within 2–4 min), a subsequent *I–V* was recorded. A small number of cells did not respond significantly to ISO, but were still included in the analysis (2 out of 22 total cells).

Elevated $[Ca^{2+}]_i$ enhances I_{Ks} amplitude and negatively shifts voltage dependence of activation in rabbit ventricular myocytes

To determine if steady-state increases in $[Ca^{2+}]_i$ regulate rabbit I_K, we recorded I_{Ks} and I_{Kr} from freshly isolated rabbit ventricular myocytes with intracellular pipette solutions that buffered free $[Ca^{2+}]_i$ to 0, 100, 300, 500, or 600 nM. From a holding potential of −50 mV, I_{Ks} was recorded by step-like square pulses from −40 to 50 mV in 10 mV increments for 3 s, followed by a tail-pulse to −50 mV for 3 s (Fig. 2*A* inset). The voltage dependence of I_{Ks} amplitude at the end of the 3 s pulse (minus a baseline that was leak-corrected for each voltage step) is shown in Fig. 2*B* (Step I_{Ks}). The *I–V* relations for tail I_{Ks} upon repolarization to −50 mV (measured as the amplitude of the decaying tail current exponential fit) are shown in Fig. 2*C*. I_{Ks} amplitudes at +50 mV (I_{MAX}) were fitted by a Hill equation ($I = I_{MAX}/(1 + (K_m/[Ca^{2+}]_i)N_H)$) as a function of $[Ca^{2+}]_i$, yielding an apparent K_m of 253 nM and Hill coefficient ($N_H = 2.4$), indicative of cooperative activation typical of CaM-dependent mechanisms (Fig. 2*D*). Boltzmann equation fits shown in Fig. 2*C* yielded the V_m for half-maximal activation ($V_{1/2}$, Fig. 2*E*) and activation slope factor (*k*, Fig. 2*F*).

When $[Ca^{2+}]_i$ was increased from 0 to 300 nM, mean I_{MAX} was more than doubled (0.60 *vs.* 0.23 pA pF^{-1}). Importantly, raising the pipette $[Ca^{2+}]_i$ from 500 to 600 nM $[Ca^{2+}]_i$ further increased I_{MAX} (0.78 or 0.82 pA pF^{-1}, respectively), and the plateau suggested an approach to saturation (Fig. 1*C* and *D*). $V_{1/2}$ was negatively shifted by ∼10 mV when I_{Ks} was recorded with high $[Ca^{2+}]_i$ of 500 and 600 nM (Fig. 2*E*), with the steepest decline consistent with the $[Ca^{2+}]_i$ dependence of I_{MAX}. The slope factor, *k*, was not significantly changed by $[Ca^{2+}]_i$ (Fig. 2*E*). I_{Ks} could not be measured using steady-state $[Ca^{2+}]_i > 600$ nM due to progressive cellular contracture and cell death. These data suggest that high $[Ca^{2+}]_i$ alters I_{Ks} by increasing I_{MAX} and shifting the V_m dependence of channel activation to more negative potentials.

To ensure that the free-Ca^{2+} of the pipette solutions were calculated correctly, $[Ca^{2+}]_i$ was monitored during electrophysiological recordings by preloading myocytes with Fluo 4-AM and including 50 μM Fluo 4-K^+ salt in the pipette solution (Fig. 3*A*). The fluorescence signal was background subtracted and fitted to a single site binding equation to determine an apparent K_d of 546 nM (Fig. 3*B*). While higher than the published K_d of Fluo-4 in aqueous solutions (335 nM), it is consistent with ∼2-fold higher K_d values for this class of Ca^{2+} indicators when directly measured in myoplasm (Harkins *et al.* 1993; Bassani *et al.* 1995). These data showed that the actual $[Ca^{2+}]_i$ in the myocytes used to measure K^+-currents were close to the predicted free $[Ca^{2+}]$ of the pipette solutions.

To confirm that CaM is involved in the $[Ca^{2+}]_i$ dependence of I_{Ks}, as is expected, we measured I_{Ks}

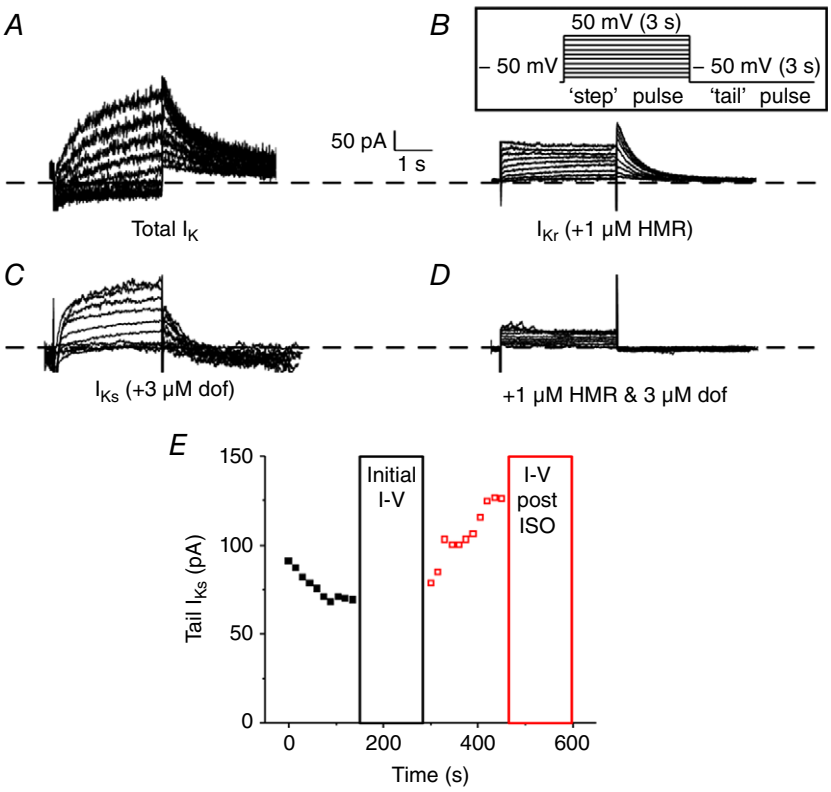

Figure 1. Distinction between I_{Ks} and I_{Kr}
A–C, representative traces of whole-cell total I_K (*A*), I_{Kr} (*B*) and I_{Ks} (*C*) measured from isolated rabbit ventricular myocytes. Currents were recorded by applying step-like pulses (inset) from −40 to 50 mV in 10 mV increments for 3 s, followed by a 'tail' pulse to −50 mV for 3 s. The inter-pulse interval was 15 s. *D*, representative traces of whole-cell currents recorded with high pipette $[Ca^{2+}]$ from the same cell as in *C* after perfusion of 1 μM HMR to show selective I_{Ks} block. *E*, an exemplar time course of tail I_{Ks} monitored before (black) and after (red) perfusion of ISO when pipette $[Ca^{2+}]$ was high.

in the absence and presence of 50 μM W7, a widely used CaM inhibitor. Figure 3*C* and *D* shows that W7 inhibited I_{Ks} measured at 500 nM $[Ca^{2+}]_i$ by approximately 50%, consistent with CaM being the mediator of the Ca^{2+}-dependent increase in I_{Ks} in Fig. 2.

Since previous studies in mammalian myocytes had only assessed $[Ca^{2+}]_i$ dependence of total I_K, rather than I_{Ks} *vs.* I_{Kr} (Tohse, 1990; Nitta *et al.* 1994), we also repeated our protocols measuring I_{Kr} to test whether rabbit ventricular I_{Kr} is sensitive to high physiological $[Ca^{2+}]_i$ (Fig. 4*A*). The *I–V* relations of tail I_{Kr} were described using a Boltzmann equation to determine I_{MAX}, $V_{1/2}$ and *k* (Fig. 4*B–E*). We concluded that rabbit I_{Kr} is not sensitive to steady-state changes in $[Ca^{2+}]_i$ because no parameters were significantly altered when I_{Kr} was recorded with $[Ca^{2+}]_i$ of 0, 100, 300, or 600 nM.

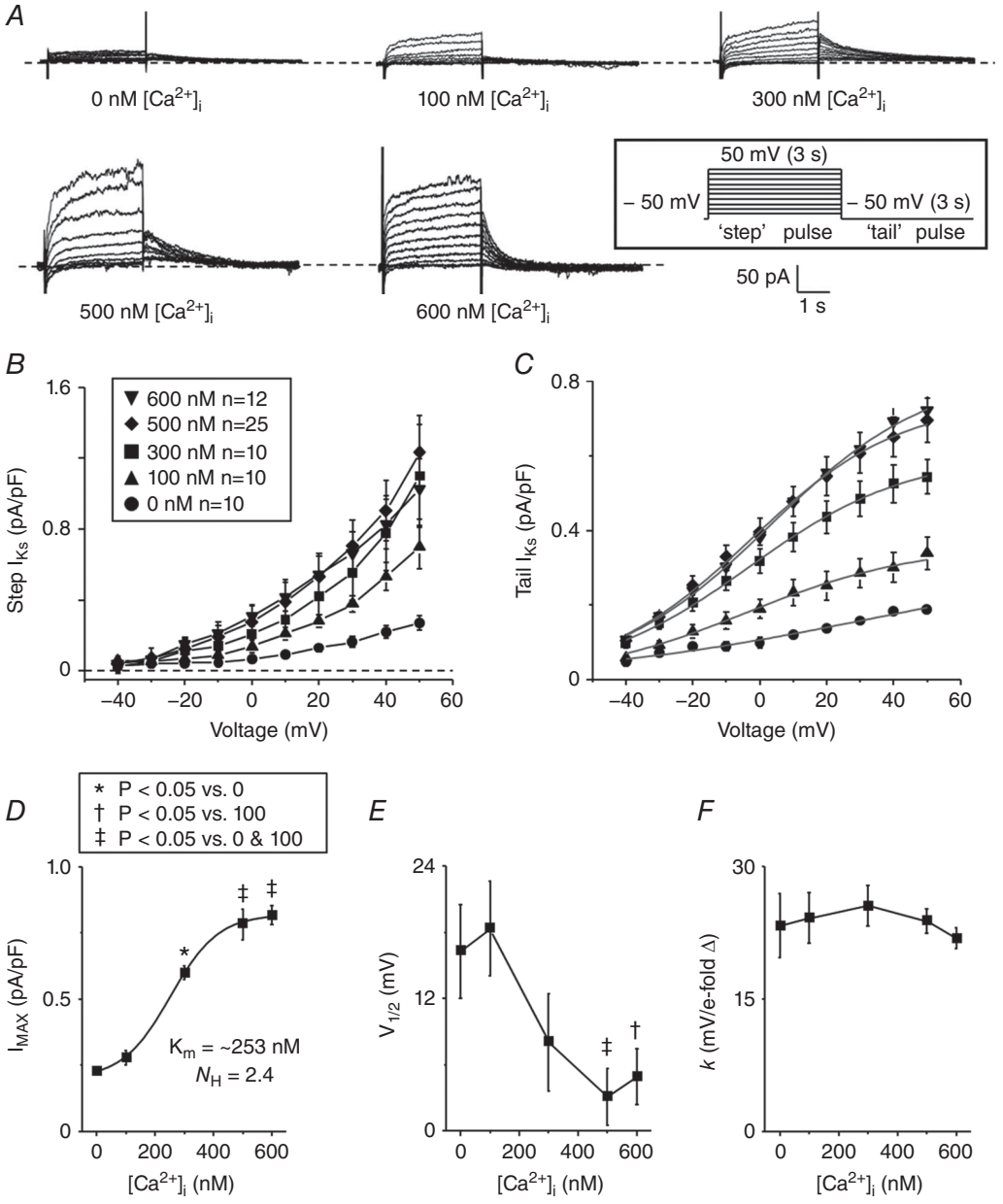

Figure 2. Assessment of steady-state Ca^{2+} dependence of I_{Ks}
A, representative traces of whole-cell I_{Ks} measured from isolated rabbit ventricular myocytes. I_{Ks} was recorded by applying the same V_m protocol as Fig. 1 (inset). *B* and *C*, the mean peak 'step' (*B*) and 'tail' (*C*) I_{Ks} are plotted as a function of the step voltage for cells recorded using a pipette solution containing free $[Ca^{2+}]_i$ of 0, 100, 300, 500, and 600 nM. *D–F*, the tail *I–V* relations were described using a Boltzmann equation (grey line, *C*) to determine I_{MAX} (*D*), $V_{1/2}$ (*E*) and *k* (*F*). For all figures, number of cells (*n*) and significance tests are indicated in boxed insets where appropriate.

Next, since β-adrenergic stimulation plays an important role in regulating I_{Ks}, we measured differences in steady-state $[Ca^{2+}]_i$ sensitivity of I_{Ks} induced by 50 nM ISO perfusion (Fig. 5). Tail *I–V* relations of I_{Ks} were plotted as a function of the step-pulse potential before and after perfusion of 50 nM ISO and described with a Boltzmann equation (Fig. 5*B* and *C*). ISO perfusion increased I_{MAX} even at zero $[Ca^{2+}]_i$, but in the presence of ISO raising $[Ca^{2+}]_i$ further increased I_{MAX}, roughly parallel to that seen in the control (CNT in Fig. 5*D*). In this series, the Ca^{2+} dependence was less sigmoidal, but the apparent half-point for Ca^{2+}-dependent I_{MAX} increase was similar plus or minus ISO (225 and 235 nM, respectively), and consistent with the K_m estimate in Fig. 2*D*. ISO perfusion also caused a negative shift in the $V_{1/2}$ for all $[Ca^{2+}]_i$ tested, but retained a roughly parallel $[Ca^{2+}]_i$ dependence

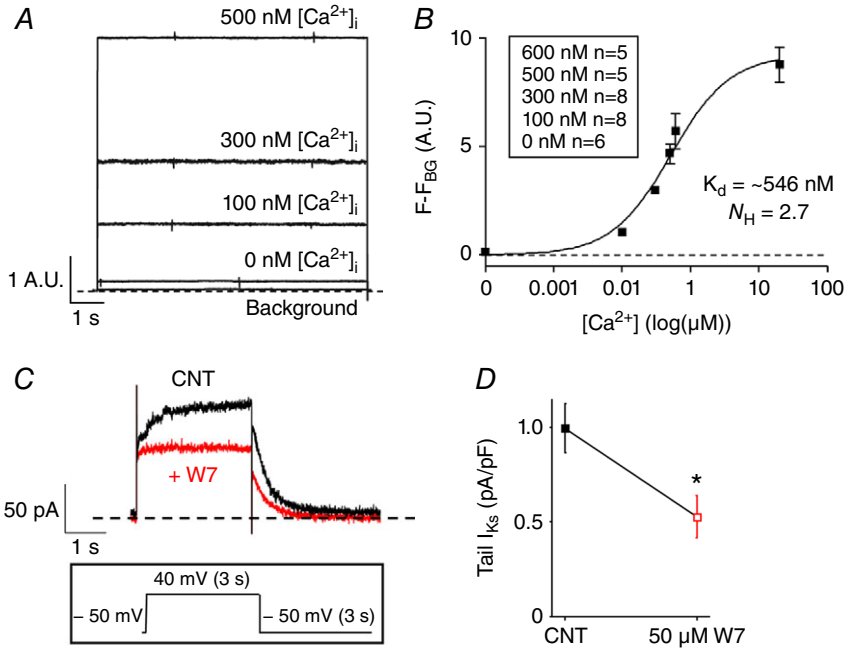

Figure 3. Representative traces of Ca^{2+}-fluorescence signal recordings during simultaneous whole-cell patch clamp measurements
A, isolated rabbit ventricular myocytes were preloaded with Fluo-4 AM and the patch pipette solution was loaded with Fluo-4 K^+ salt. The Ca^{2+} signal was recorded for 0, 100, 300, 500 and 600 nM $[Ca^{2+}]_i$ using the same V_m protocol as in Fig. 1. *B*, the fluorescence signal was background subtracted and fitted to a single site binding equation. *C*, representative traces of I_{Ks} recorded with pipette $[Ca^{2+}]$ 500 nM before (black) and after (red) perfusion of 50 μM W7. I_{Ks} was recorded by applying a step pulse from −50 to 40 mV for 3 s, followed by a tail pulse to −50 mV for 3 s (inset). *D*, the bar graph represents the mean peak tail I_{Ks} recorded before or after W7 perfusion ($n = 5$, $P < 0.05$).

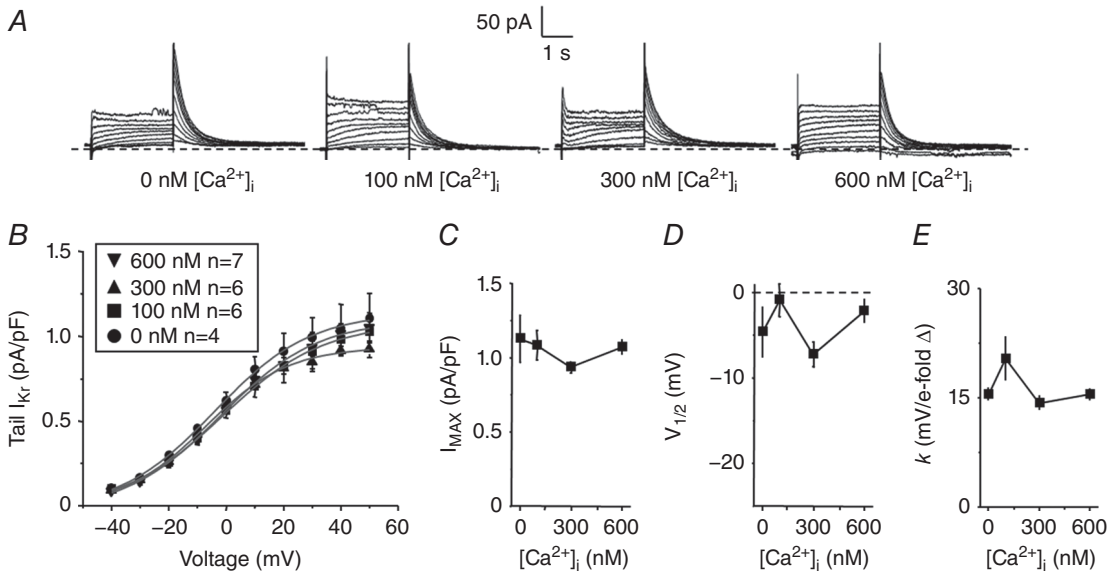

Figure 4. Assessment of steady-state Ca^{2+} dependence of I_{Kr}
A, representative traces of whole-cell I_{Kr} measured from isolated rabbit ventricular myocytes. The same V_m protocol was used as in Fig. 1. *B*, the mean peak tail I_{Kr} are plotted as a function of the step voltage for cells recorded using a pipette solution containing free $[Ca^{2+}]_i$ of 0, 100, 300 and 600 nM. *C–E*, the tail *I–V* relations were described using a Boltzmann equation (grey line, Fig. 4*B*) to determine I_{MAX} (*C*), $V_{1/2}$ (*D*) and *k* (*E*).

(Fig. 5*E*). Neither ISO nor $[Ca^{2+}]_i$ altered *k* significantly (Fig. 5*F*). Thus, ISO does not appreciably alter the $[Ca^{2+}]_i$ dependence of I_{Ks}.

Additionally, activation kinetics, τ_{act}, were fitted to a single exponential during the 40 mV test pulse and were unchanged by ISO (Fig. 6*A* and *B*). The tail current at −50 mV following a 40 mV test pulse was fitted to a single exponential to determine τ_{deact}. Both ISO and $[Ca^{2+}]_i$ slowed deactivation kinetics of tail I_{Ks}, and appeared additive, based on the similar shapes of the curves (Fig. 6*C*). These results indicate that in rabbit both elevated $[Ca^{2+}]_i$ and β-adrenergic stimulation increase I_{Ks} amplitude, negatively shift $V_{1/2}$ and slow deactivation kinetics. And the effects of $[Ca^{2+}]_i$ and ISO are phenotypically similar, but appear additive. That is, even at a $[Ca^{2+}]_i$ that seems maximal with respect to $[Ca^{2+}]_i$, ISO still causes a further change in I_{MAX}, $V_{1/2}$ and deactivation.

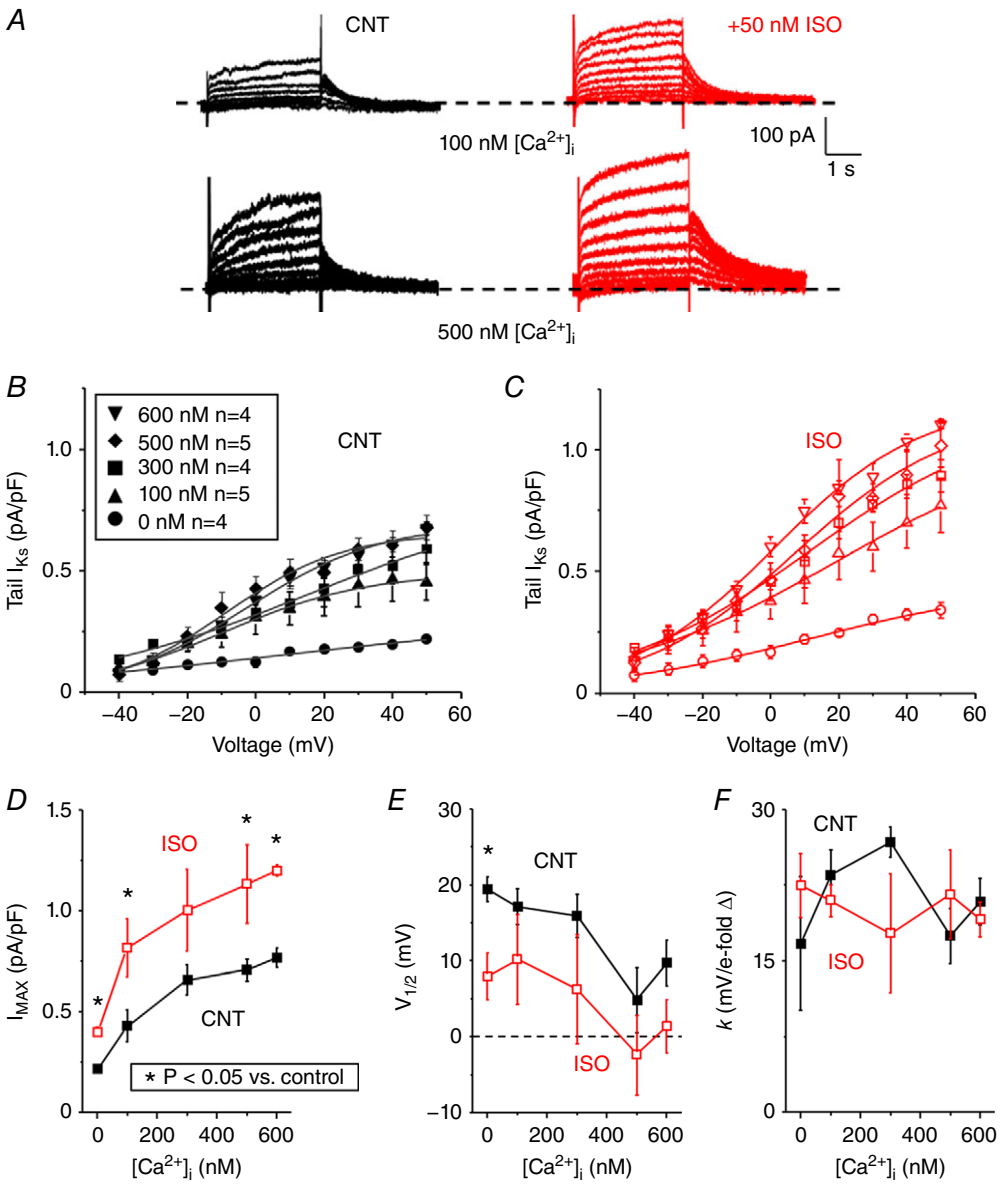

Figure 5. ISO and $[Ca^{2+}]_i$ increase I_{MAX} of I_{Ks}
A, representative traces of I_{Ks} measured from isolated rabbit ventricular myocytes at room temperature before (black) and after (red) 50 nM [ISO] perfusion for pipette solutions containing $[Ca^{2+}]_i$ of 100 and 500 nM. The same V_m protocol was used as in Fig. 1. *B* and *C*, the mean peak tail I_{Ks} before (*B*) and after (*C*) ISO are plotted as a function of step voltage for cells recorded with a pipette solution containing free $[Ca^{2+}]_i$ of 0, 100, 300, 500, or 600 nM. *D–F*, the tail *I–V* relations were described using a Boltzmann equation (grey line, Fig. 5*B* and *C*) to determine I_{MAX} (*D*), $V_{1/2}$ (*E*) and *k* (*F*).

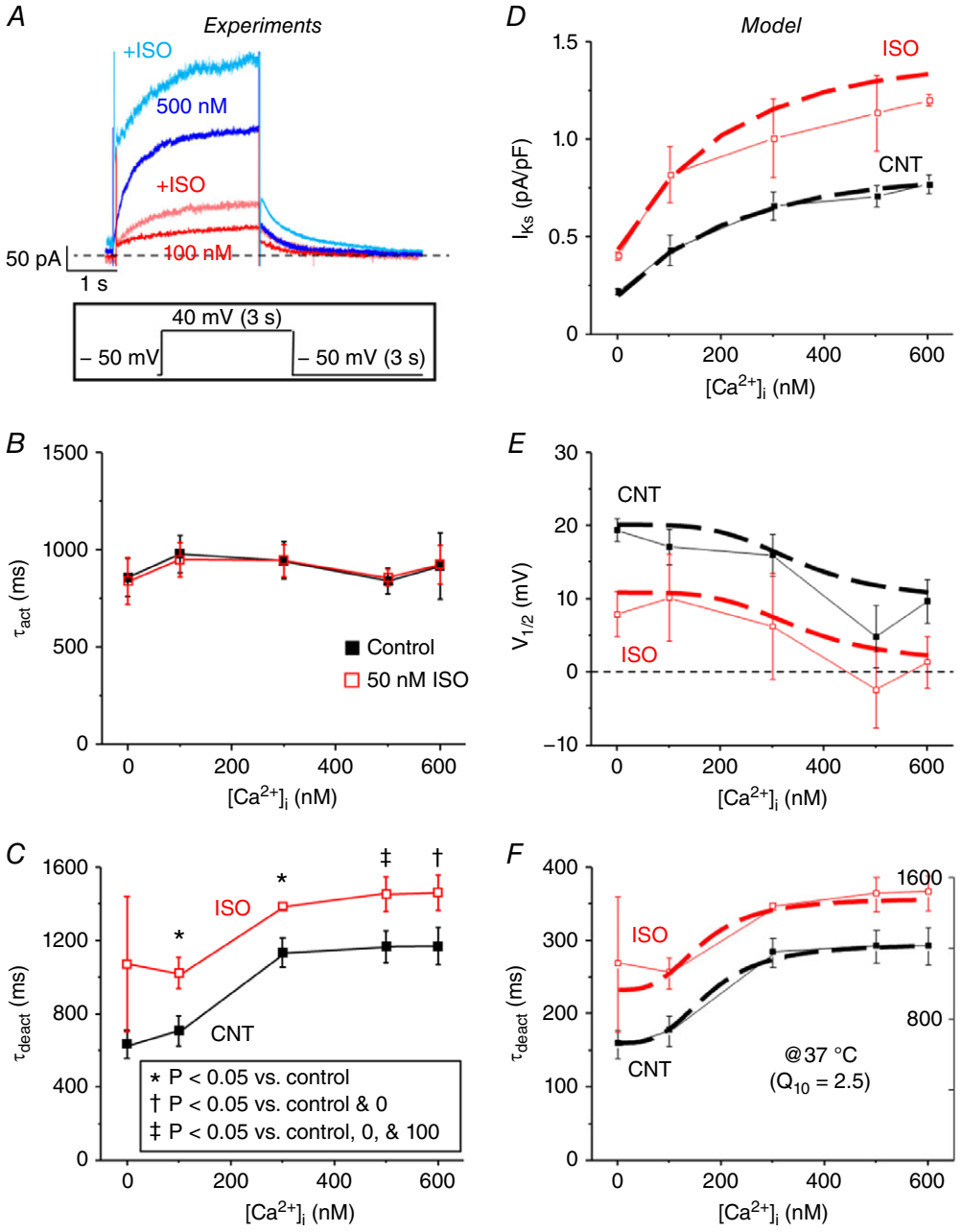

Figure 6. $[Ca^{2+}]_i$ slows deactivation of I_{Ks}
A, representative traces of I_{Ks} recorded using pipette solutions with free $[Ca^{2+}]_i$ of 100 and 500 nM before (100 nM, red; 500 nM, blue) and after (100 nM, light red; 500 nM, light blue) ISO are overlaid. I_{Ks} was recorded using the same V_m protocol as in Fig. 3*C* by applying a step pulse from −50 to 40 mV for 3 s, followed by a tail pulse to −50 mV for 3 s. *B*, τ_{act} of I_{Ks} was fitted to a single exponential during the step pulse to 40 mV and is plotted as a function of free $[Ca^{2+}]_i$ in the pipette solution before (black) and after (red) ISO perfusion for 0, 100, 300, 500, and 600 nM $[Ca^{2+}]_i$. *C*, the decay in tail I_{Ks} following the 40 mV step-pulse was fitted to a single exponential to determine τ_{deact} and is plotted as a function of free $[Ca^{2+}]_i$ in the pipette solution before and after ISO perfusion for 0, 100, 300, 500, and 600 nM $[Ca^{2+}]_i$. The n values for each situation are the same as in Fig. 5. The $[Ca^{2+}]_i$ dependence and ISO effects (50 nM) on I_{Ks} (*D*), $V_{1/2}$, (*E*) and τ_{deact} (*F*) were incorporated into a model of I_{Ks} based on the experimental data and was scaled to 37 °C. Simulated I_{Ks} (dashed lines) are shown overlaid with experimental results (solid lines).

I_{Ks} increases during an AP with high buffered $[Ca^{2+}]_i$ and during physiological Ca^{2+} transients

Figure 6*D–F* shows how our updated I_{Ks} model recapitulates our experimental results, with respect to the Ca^{2+} and ISO dependence of current amplitude, voltage dependence, and deactivation kinetics. During AP-clamp simulations at 1 Hz we further tested how normal CaTs *vs.* $[Ca^{2+}]_i$ clamping affected I_{Ks} (Fig. 7*A–C*). When $[Ca^{2+}]_i$ was clamped at 100 nM, I_{Ks} was small, but I_{Ks} was ~3-fold larger when $[Ca^{2+}]_i$ was clamped at 500 nM. When $[Ca^{2+}]_i$ was unbuffered, which allowed normal dynamic CaTs, I_{Ks} was nearly identical to the 500 nM simulations (Fig. 7*B*). This seemed somewhat surprising, because the peak submembrane and cleft $[Ca^{2+}]_i$ where the potassium channels reside rises much higher (~12 and 220 μM, respectively, in the model), far exceeding the $[Ca^{2+}]_i$ used

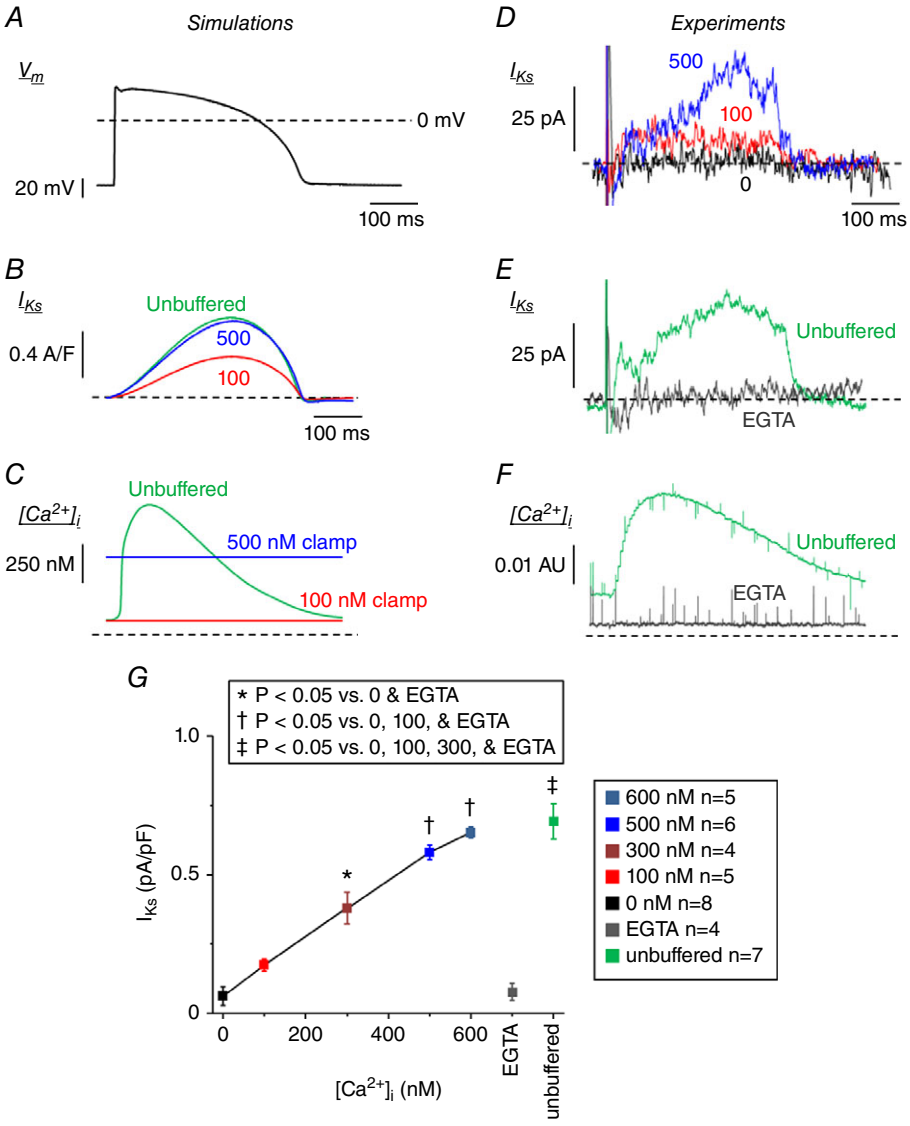

Figure 7. Ca^{2+} dependence of HMR-sensitive I_{Ks} activated during AP waveform
A, rabbit ventricular AP waveform used for AP simulations and to record HMR-1556-sensitive I_{Ks} at 35–37°C. *B* and *C*, time courses of I_{Ks} (*B*) and CaT (*C*) during 1 Hz computational simulations using the AP waveform as in Fig. 7*A* are shown with $[Ca^{2+}]_i$ clamped at 100 (red) and 500 nM (blue), or unbuffered (Free CaT, green). *D*, representative whole-cell current subtracted HMR-sensitive (1 μM) I_{Ks} traces are overlaid for cells recorded with free $[Ca^{2+}]_i$ of 0 (black), 100 (red) and 500 nM (blue). *E*, representative whole-cell current subtracted HMR-sensitive (1 μM) I_{Ks} traces are overlaid for cells recorded (using the AP waveform in Fig. 7*A* as the V_m command) with $[Ca^{2+}]_i$ heavily buffered by 10 mM EGTA (grey) or unbuffered (green). *F*, the corresponding Ca^{2+} signal is shown. Note that free $[Ca^{2+}]_i$ is reduced at baseline and during the AP when buffered, and a normal CaT is present when unbuffered. *G*, the peak I_{Ks} during ventricular AP waveform recordings are plotted for cells recorded using a pipette solution containing free $[Ca^{2+}]_i$ of 0, 100, 300, 500, or 600 nM, and buffered with EGTA or unbuffered.

in the $[Ca^{2+}]_i$-clamp experiments. This would suggest that in myocytes I_{Ks} is typically maximally Ca^{2+}-activated at $[Ca^{2+}]_i$ > 600 nM, which would virtually always occur during the AP in the submembrane and cleft domains. The only noticeable difference in the unbuffered and 500 nM curves in Fig. 7*B* is that I_{Ks} declines slightly faster in the unbuffered case, consistent with the declining CaT at that time (between the 100 and 500 nM clamp curves in Fig. 7*C*).

To explore these *in silico* inferences experimentally, we measured I_{Ks} during AP-clamp conditions (Fig. 7*D*–*G*) using a typical rabbit ventricular AP waveform recorded from freshly isolated rabbit ventricular myocytes at 35–37°C. HMR-1556 (1 μM) was used to isolate I_{Ks} as the HMR-sensitive current activated during the AP. We again used pipette solutions with free $[Ca^{2+}]_i$ clamped at 0, 100, 300, 500 and 600 nM (now at physiological temperature; Fig. 7*D* and *G*). Similar to the room temperature experiments (Figs 1–6), the HMR-sensitive I_{Ks} increased in a $[Ca^{2+}]$-dependent manner (Fig. 7*G*). The Ca^{2+} dependence was less obviously saturating at 600 nM (*vs.* Figs 2*D* and 5*D*), but the I_{Ks} at 300 nM was ~60% of that at 600 nM $[Ca^{2+}]_i$.

In this experimental series we also used pipette solutions that were either unbuffered (no BAPTA or dibromo-BAPTA), which allows normal CaTs to occur, or heavily buffered with 10 mM EGTA, i.e. similar to the 0 nM $[Ca^{2+}]_i$ BAPTA-based solution (Fig. 7*E*). $[Ca^{2+}]_i$ was monitored again using Fluo 4-AM and 50 μM Fluo 4-K^+ salt in the pipette to detect either a normal CaT during the AP (unbuffered) or a flat Ca^{2+} signal with 10 mM EGTA (Fig. 7*F*). Figure 7*G* shows that the peak I_{Ks} during the AP in the unbuffered case was similar to that in the 600 nM $[Ca^{2+}]_i$-clamp case. These data are consistent with the model prediction and suggest that I_{Ks} is maximally activated when $[Ca^{2+}]_i$ reaches > 500 nM, and that that condition is met during the normal CaT. We examined for, but could not detect any kinetic differences (e.g. I_{Ks} in the unbuffered case being higher early and lower late), which is likely to be because noise levels and cell–cell variations in these small difference-currents limited resolution of such kinetic differences.

Functional consequences of Ca^{2+} and ISO dependence of I_{Ks}

To assess the impact and potential synergy of Ca^{2+} and ISO dependence of I_{Ks} on AP repolarization, Fig. 8 shows simulations at a fast rate (3 Hz) in the absence of ISO and in the presence of either 20 nM ISO (submaximal) or 50 nM (near-maximal and as used in experiments). During β-adrenergic activation, the increase in I_{Ks} is mostly a consequence of PKA phosphorylation, because the effect of $[Ca^{2+}]_i$ augmentation on I_{Ks} is already near maximal in control. That is, the higher CaT amplitude with ISO does not further increase I_{Ks}. Importantly, our results show evident I_{Ks} enhancement at this fast rate, and particularly, the slowed deactivation kinetics enhance instantaneous I_{Ks} at the start of the subsequent AP. This factor gives I_{Ks} a

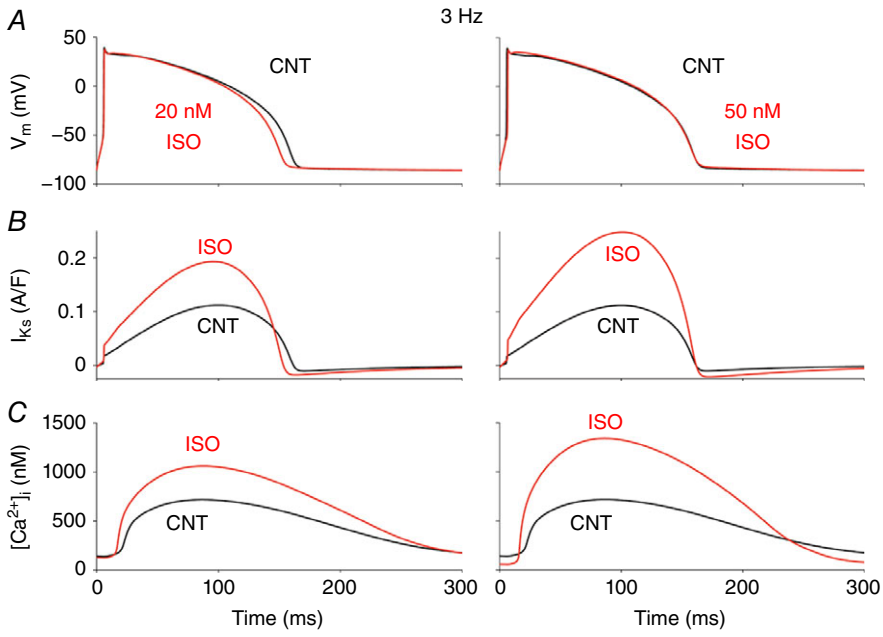

Figure 8. Ca^{2+} and ISO dependence of I_{Ks} contribute to rabbit ventricular AP shortening during β-AR stimulation
Simulated time courses of membrane potential, V_m (*A*), I_{Ks} (*B*) and CaT (*C*) during steady-state 3 Hz pacing are shown before (black) and after (red) ISO (20 nM, left; and 50 nM, right).

head-start during the AP, ensuring that at high heart rates and shorter AP duration, I_{Ks} can limit AP prolongation (together with PKA effects at other targets, e.g. I_{CaL} and PLM; Negroni *et al.* 2015).

Discussion

Many studies over the past several decades have shown how Ca^{2+} can directly or indirectly influence ion channel function in the heart, neurons, epithelial tissue and other important regions of the body. In contractile cells, such as cardiomyocytes, studying these mechanisms is technically difficult, because high levels of $[Ca^{2+}]_i$ lead to contraction or cell death during recordings, and thus data acquisition is challenging. This is the first study to dissect the Ca^{2+} dependence of both I_{Ks} and I_{Kr} in rabbit ventricular myocytes and to provide direct evidence that $[Ca^{2+}]_i$ is critical for I_{Ks} function during a rabbit ventricular AP.

Key novel findings here are the following: (1) $[Ca^{2+}]_i$ in the physiological range (K_m ~250 nM) dynamically regulates I_{Ks} (and not I_{Kr}). (2) The $[Ca^{2+}]_i$-dependent effects are quite similar to those of ISO, in the extent to which they increase I_{Ks} amplitude, negatively shift $V_{1/2}$ of activation, and slow deactivation. Likewise, neither an increase in $[Ca^{2+}]_i$ nor β-AR activation alter the slope of V_m dependence activation (k) or τ_{act}. (3) The effects of increased $[Ca^{2+}]_i$ and ISO are additive and both contribute to increase I_{Ks} during β-AR activation. (4) During the physiological AP and CaT, Ca^{2+}-dependent activation of I_{Ks} is nearly maximal, even in the absence of ISO. These observations from experimental data were recapitulated *in silico*, and together suggest that although Ca^{2+} is critical for normal I_{Ks} function, I_{Ks} reaches a maximal amplitude at $[Ca^{2+}]_i$ of ~600 nM. Importantly, our experimental and simulated results suggest that I_{Ks} kinetics are quite similar when $[Ca^{2+}]_i$ is buffered at high concentrations or when $[Ca^{2+}]_i$ is cycling in the cell during a CaT.

It has been estimated that ion channels at the sarcolemma 'sense' $[Ca^{2+}]_i$ in the micromolar range during the initial milliseconds of a normal CaT during myocyte contraction, and in our simulations the $[Ca^{2+}]$ in the submembrane space reaches > 10 μM (Weber *et al.* 2002; Negroni *et al.* 2015). Our results suggest that Ca^{2+} regulates I_{Ks} with sufficiently high affinity that this regulation is saturated at all submembrane $[Ca^{2+}]_i$ levels that are likely to occur physiologically during each beat. We had hoped to assess the kinetics of Ca^{2+}-dependent activation during the physiological CaTs, where some cells showed rapid I_{Ks} activation (as in the exemplar in Fig. 7*E*). However, cell-to-cell variability and the small current size prevented unequivocal distinction with respect to the early phase of I_{Ks} with SR Ca^{2+} release *vs.* $[Ca^{2+}]_i$ clamp at 500 nM. The modelling simulations in Fig. 7*B* illustrate that the theoretical difference is expected to be quite small.

Comparison with previous studies

Previous studies have assessed the Ca^{2+} dependence of I_K in guinea pig ventricular myocytes by whole-cell and excised patches (Tohse, 1990; Nitta *et al.* 1994). Both studies showed that I_K increased in a concentration-dependent manner with increasing $[Ca^{2+}]_i$ with slightly higher affinity than our results (K_m ~38 nM, N_H = 1.4 in Nitta *et al.* 1994 *vs* 253 nM, N_H = 2.4). Note, that Tohse (1990) tested only up to 100 nM $[Ca^{2+}]_i$. Most modern AP models have used a K_m for I_{Ks} $[Ca^{2+}]_i$ dependence of either 38 or 63 nM (Zeng *et al.* 1995; Negroni *et al.* 2015). We have now updated the I_{Ks} model within Negroni *et al.* (2015) to fit our present data. Nitta *et al.* (1994) found a negative shift in the $V_{1/2}$ of I_K activation while Tohse (1990) did not. These studies provide evidence that I_K could limit Ca^{2+} entry by accelerating repolarization and subsequently promoting Ca^{2+} extrusion from the cytosol. However, the Ca^{2+} sensitivity was never distinguished between I_{Kr} and I_{Ks}, and I_{Ks} amplitude and kinetics in guinea pig differ greatly from larger mammals such as rabbit, dog and human (Jost *et al.* 2007; Bartos *et al.* 2015). Our results clearly distinguish that rabbit I_{Ks} is highly Ca^{2+} sensitive, but I_{Kr} is not. We also show that the voltage dependence of I_{Ks} was negatively shifted and deactivation kinetics were slowed by high $[Ca^{2+}]_i$, consistent with previous findings.

I_{Ks} increases in a Ca^{2+}-dependent manner, but I_{Kr} is larger at all $[Ca^{2+}]_i$ tested here and is the key outward current during normal rabbit ventricular repolarization. However, I_{Ks} reaches an amplitude similar to I_{Kr} subsequent to ISO perfusion when recorded with high $[Ca^{2+}]_i$, thus highlighting the importance of β-adrenergic regulation of I_{Ks}. These observations align with dynamic clamp recordings in guinea pig myocytes made while maintaining physiological $[Ca^{2+}]_i$ cycling, whereby I_{Ks} is larger than I_{Kr} subsequent to β-adrenergic stimulation (Banyasz *et al.* 2014). Regardless of ISO perfusion, rabbit I_{Ks} increases ~3.5-fold when $[Ca^{2+}]_i$ is increased from 0 to 500–600 nM. Importantly, at all Ca^{2+} concentrations ISO perfusion still led to an increase of I_{Ks} by ~2× (Fig. 9). These results resemble the original I_K observations in guinea pig ventricular myocytes, where even with PKA or PKC activity inhibited, I_K remained augmented at elevated $[Ca^{2+}]$ (Nitta *et al.* 1994). We conclude that β-adrenergic activation is able to stimulate I_{Ks} in a manner independent of $[Ca^{2+}]_i$; however, the similar (and additive) effects might imply a common molecular shift. Specifically, several studies showed how PKA phosphorylation at S27 on the N-terminus of Kv7.1 leads to a reduction in drug sensitivity suggesting that PKA phosphorylation restricts allosteric drug binding because of changes in the molecular conformation of Kv7.1 (Yang *et al.* 2009, 2013; Bartos *et al.* 2014). The ISO- and Ca^{2+}-dependent changes in I_{Ks} biophysical properties are similar, and these effects

may influence the voltage-sensing and pore domains in a comparable fashion. However, the ISO-dependent process may originate in the N-terminus and the Ca^{2+} dependency may act via direct binding to CaM on the C-terminus of Kv7.1.

When using high $[Ca^{2+}]_i$, it is noteworthy that both main ventricular myocyte isoforms of adenylyl cyclase (AC; AC5 in adult and AC6 in neonate) are partially inhibited by high $[Ca^{2+}]_i$, in part by competing with Mg^{2+}-dependent activation (Hu *et al.* 2002). Over the physiological range of $[Ca^{2+}]_i$ and $[Mg^{2+}]_i$, this may limit, but not prevent, AC activation by β-adrenergic agonists. Indeed, there is little question that β_1-adrenergic activation strongly activates both cAMP production and PKA activity in cardiac myocytes despite a concurrent rise in $[Ca^{2+}]_i$ that might temper AC5 activation. Furthermore, the fact that the curves in Fig. 5*D* are relatively parallel demonstrates that the high $[Ca^{2+}]_i$ is not preventing β-adrenergic-dependent increase in I_{Ks} at that $[Ca^{2+}]_i$. This tells us that the physiologically resulting effect of these two activating effects predominate over Ca^{2+}-dependent AC inhibition. It is conceivable that the apparent slight decrease in percentage increase of I_{Ks} by ISO at higher $[Ca^{2+}]_i$ (Fig. 9, red curve) might reflect this AC effect, but that is only speculation.

Ca^{2+} regulation of I_{Ks} involves proper binding of CaM to the Kv7.1 macromolecular complex

Reports of LQT1 mutants in IQ motifs of Kv7.1 and structural modelling insight suggest that CaM is required for proper I_{Ks} function in native and heterologous systems (Nitta *et al.* 1994; Bai *et al.* 2005; Ghosh *et al.* 2006; Shamgar *et al.* 2006; Sachyani *et al.* 2014). Mutants that disrupt the IQ motifs critical for CaM binding to the C-terminus of Kv7.1 or engineered mutations that disrupt the EF hand on the N-lobe of CaM (rendering the N-lobe of CaM Ca^{2+}-insensitive) suggest that CaM is constitutively bound to Kv7.1 and Ca^{2+} dependency of I_{Ks} is a CaM-dependent process (Ghosh *et al.* 2006; Shamgar *et al.* 2006; Sachyani *et al.* 2014). When Kv7.1–CaM interactions are disrupted, I_{Ks} is largely reduced and the voltage dependence of activation is positively shifted. Furthermore, we found that rabbit I_{Ks} recorded with high $[Ca^{2+}]_i$ (500 nM) was inhibited by 50% following perfusion of W7, a CaM antagonist (Figure 3*C*). These studies and our results suggest that Ca^{2+} sensitivity of I_{Ks} is a CaM-mediated process, with an apparent K_m in the physiological $[Ca^{2+}]_i$ range.

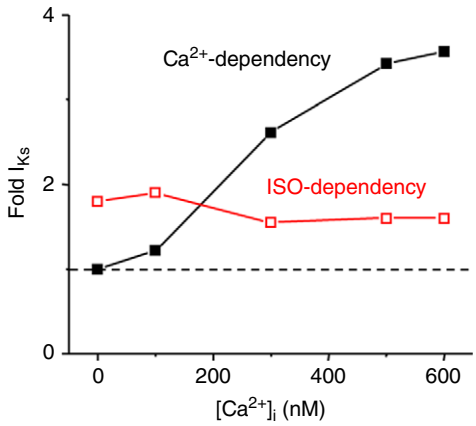

Figure 9. Effects of Ca^{2+} and ISO dependence of rabbit I_{Ks}
Dashed line represents I_{Ks} amplitude under control conditions when $[Ca^{2+}]_i$ is highly buffered essentially to 0 in the pipette solution (based on data in Fig. 5*D*).

Physiological impact of the Ca^{2+} dependence of I_{Ks}

It is likely that the negative shift in voltage dependence of activation and postponed deactivation of rabbit I_{Ks} contribute to the increase in current amplitude subsequent to a rise in $[Ca^{2+}]_i$, as replicated by our mathematical model. Recent studies have showed that an elevation in $[Ca^{2+}]_i$ or cellular stress leads to higher co-localization of Kv7.1 with KCNE1 at the sarcolemma of guinea pig ventricular myocytes, which one would expect to result in increased I_{Ks} (Wang *et al.* 2013). Alterations in Kv7.1 protein expression at the cell surface were not assessed in our study, but rapid increases in surface expression could conceivably contribute to the overall Ca^{2+}-induced increase in rabbit I_{Ks} density.

Our simulation results suggest that during β-adrenergic activation both Ca^{2+} increase and PKA-dependent phosphorylation contribute to I_{Ks} enhancement that tends to abbreviate the cardiac AP. Although speculative, our data and other studies support the concept that Ca^{2+} sensitivity of I_{Ks} is crucial for the repolarization reserve during situations when cells are overloaded with Ca^{2+}, for example during heart failure.

Clinical significance

In heart failure, impaired $[Ca^{2+}]_i$ dynamics (elevated diastolic $[Ca^{2+}]_i$ and attenuated CaT) and AP prolongation are a common observation in cellular pathophysiology. Here, we show that normal CaTs are necessary for normal I_{Ks} function, and suppression of $[Ca^{2+}]_i$ leads to reduced I_{Ks}. This may suggest that pathological AP prolongation and Ca^{2+}-loading favours the role of I_{Ks} during repolarization. Therapeutic strategies designed to restore normal $[Ca^{2+}]_i$ dynamics and regulation of ion channel function, specifically Ca^{2+}-dependent channels like I_{Ks}, may prevent the occurrence of lethal arrhythmias and lead to a retention of the repolarization reserve in patients with heart failure.

Conclusions

We have shown that increasing $[Ca^{2+}]_i$ from 0 to 600 nM in rabbit ventricular myocytes increased maximally activated I_{Ks}, negatively shifted I_{Ks} voltage dependence of activation, and slowed deactivation kinetics, similar to β-adrenergic stimulation, without affecting I_{Kr} properties. During a physiological AP and CaT, measured and simulated I_{Ks} were comparable to that measured or simulated when $[Ca^{2+}]_i$ was buffered at 500–600 nM, suggesting that Ca^{2+} regulation of I_{Ks} is saturated at high submembrane $[Ca^{2+}]_i$ that occurs normally during the CaT. For the first time, this study distinguishes the Ca^{2+} dependence of I_{Ks} and I_{Kr} and provides direct measurement of the role of $[Ca^{2+}]_i$ in shaping I_{Ks} function during a rabbit ventricular AP.

References

Bai CX, Namekata I, Kurokawa J, Tanaka H, Shigenobu K & Furukawa T (2005). Role of nitric oxide in Ca^{2+} sensitivity of the slowly activating delayed rectifier K^+ current in cardiac myocytes. *Circ Res* **96**, 64–72.

Bai CX, Takahashi K, Masumiya H, Sawanobori T & Furukawa T (2004). Nitric oxide-dependent modulation of the delayed rectifier K^+ current and the L-type Ca^{2+} current by ginsenoside Re, an ingredient of *Panax* ginseng, in guinea-pig cardiomyocytes. *Br J Pharmacol* **142**, 567–575.

Banyasz T, Horvath B, Jian Z, Izu LT & Chen-Izu Y (2011). Sequential dissection of multiple ionic currents in single cardiac myocytes under action potential-clamp. *J Mol Cell Cardiol* **50**, 578–581.

Banyasz T, Jian Z, Horvath B, Khabbaz S, Izu LT & Chen-Izu Y (2014). Beta-adrenergic stimulation reverses the I_{Kr}–I_{Ks} dominant pattern during cardiac action potential. *Pflugers Arch* **466**, 2067–2076.

Barhanin J, Lesage F, Guillemare E, Fink M, Lazdunski M & Romey G (1996). K_VLQT1 and lsK (minK) proteins associate to form the I_{Ks} cardiac potassium current. *Nature* **384**, 78–80.

Bartos DC, Giudicessi JR, Tester DJ, Ackerman MJ, Ohno S, Horie M, Gollob MH, Burgess DE & Delisle BP (2014). A KCNQ1 mutation contributes to the concealed type 1 long QT phenotype by limiting the Kv7.1 channel conformational changes associated with protein kinase A phosphorylation. *Heart Rhythm* **11**, 459–468.

Bartos DC, Grandi E & Ripplinger CM (2015). Ion channels in the heart. *Compr Physiol* **5**, 1423–1464.

Bassani JW, Bassani RA & Bers DM (1995). Calibration of indo-1 and resting intracellular $[Ca]_i$ in intact rabbit cardiac myocytes. *Biophys J* **68**, 1453–1460.

Bers DM (2002). Cardiac excitation-contraction coupling. *Nature* **415**, 198–205.

El-Sherif N, Chinushi M, Caref EB & Restivo M (1997). Electrophysiological mechanism of the characteristic electrocardiographic morphology of torsade de pointes tachyarrhythmias in the long-QT syndrome: detailed analysis of ventricular tridimensional activation patterns. *Circulation* **96**, 4392–4399.

Ghosh S, Nunziato DA & Pitt GS (2006). KCNQ1 assembly and function is blocked by long-QT syndrome mutations that disrupt interaction with calmodulin. *Circ Res* **98**, 1048–1054.

Goldenberg I, Thottathil P, Lopes CM, Moss AJ, McNitt S, O-Uchi J, Robinson JL, Zareba W, Ackerman MJ, Kaufman ES, Towbin JA, Vincent M & Barsheshet A (2012). Trigger-specific ion-channel mechanisms, risk factors, and response to therapy in type 1 long QT syndrome. *Heart Rhythm* **9**, 49–56.

Grandi E, Pasqualini FS & Bers DM (2010). A novel computational model of the human ventricular action potential and Ca transient. *J Mol Cell Cardiol* **48**, 112–121.

Harkins AB, Kurebayashi N & Baylor SM (1993). Resting myoplasmic free calcium in frog skeletal muscle fibers estimated with fluo-3. *Biophys J* **65**, 865–881.

Heath BM & Terrar DA (1996). The deactivation kinetics of the delayed rectifier components I_{Kr} and I_{Ks} in guinea-pig isolated ventricular myocytes. *Exp Physiol* **81**, 605–621.

Heijman J, Spatjens RL, Seyen SR, Lentink V, Kuijpers HJ, Boulet IR, de Windt LJ, David M & Volders PG (2012). Dominant-negative control of cAMP-dependent I_{Ks} upregulation in human long-QT syndrome type 1. *Circ Res* **110**, 211–219.

Hu B, Nakata H, Gu C, De Beer T & Cooper DM (2002). A critical interplay between Ca^{2+} inhibition and activation by Mg^{2+} of AC5 revealed by mutants and chimeric constructs. *J Biol Chem* **277**, 33139–33147.

Jost N, Papp JG & Varro A (2007). Slow delayed rectifier potassium current (I_{Ks}) and the repolarization reserve. *Ann Noninvasive Electrocardiol* **12**, 64–78.

Jost N, Virag L, Bitay M, Takacs J, Lengyel C, Biliczki P, Nagy Z, Bogats G, Lathrop DA, Papp JG & Varro A (2005). Restricting excessive cardiac action potential and QT prolongation: a vital role for I_{Ks} in human ventricular muscle. *Circulation* **112**, 1392–1399.

Li GR, Feng J, Yue L, Carrier M & Nattel S (1996). Evidence for two components of delayed rectifier K^+ current in human ventricular myocytes. *Circ Res* **78**, 689–696.

Liu DW & Antzelevitch C (1995). Characteristics of the delayed rectifier current (I_{Kr} and I_{Ks}) in canine ventricular epicardial, midmyocardial, and endocardial myocytes. A weaker I_{Ks} contributes to the longer action potential of the M cell. *Circ Res* **76**, 351–365.

Marx SO, Kurokawa J, Reiken S, Motoike H, D'Armiento J, Marks AR & Kass RS (2002). Requirement of a macromolecular signaling complex for β adrenergic receptor modulation of the KCNQ1-KCNE1 potassium channel. *Science* **295**, 496–499.

Negroni JA, Morotti S, Lascano EC, Gomes AV, Grandi E, Puglisi JL & Bers DM (2015). β-adrenergic effects on cardiac myofilaments and contraction in an integrated rabbit ventricular myocyte model. *J Mol Cell Cardiol* **81**, 162–175.

Nerbonne JM & Kass RS (2005). Molecular physiology of cardiac repolarization. *Physiol Rev* **85**, 1205–1253.

Nitta J, Furukawa T, Marumo F, Sawanobori T & Hiraoka M (1994). Subcellular mechanism for Ca^{2+}-dependent enhancement of delayed rectifier K^+ current in isolated membrane patches of guinea pig ventricular myocytes. *Circ Res* **74**, 96–104.

Pogwizd SM, Qi M, Yuan W, Samarel AM & Bers DM (1999). Upregulation of Na^+/Ca^{2+} exchanger expression and function in an arrhythmogenic rabbit model of heart failure. *Circ Res* **85**, 1009–1019.

Pogwizd SM, Schlotthauer K, Li L, Yuan W & Bers DM (2001). Arrhythmogenesis and contractile dysfunction in heart failure: Roles of sodium-calcium exchange, inward rectifier potassium current, and residual β-adrenergic responsiveness. *Circ Res* **88**, 1159–1167.

Sachyani D, Dvir M, Strulovich R, Tria G, Tobelaim W, Peretz A, Pongs O, Svergun D, Attali B & Hirsch JA (2014). Structural basis of a Kv7.1 potassium channel gating module: studies of the intracellular c-terminal domain in complex with calmodulin. *Structure* **22**, 1582–1594.

Salata JJ, Jurkiewicz NK, Jow B, Folander K, Guinosso PJ Jr, Raynor B, Swanson R & Fermini B (1996). I_K of rabbit ventricle is composed of two currents: evidence for I_{Ks}. *Am J Physiol Heart Circ Physiol* **271**, H2477–H2489.

Sanguinetti MC, Curran ME, Zou A, Shen J, Spector PS, Atkinson DL & Keating MT (1996). Coassembly of K_VLQT1 and minK (IsK) proteins to form cardiac I_{Ks} potassium channel. *Nature* **384**, 80–83.

Sanguinetti MC & Jurkiewicz NK (1990). Two components of cardiac delayed rectifier K^+ current. Differential sensitivity to block by class III antiarrhythmic agents. *J Gen Physiol* **96**, 195–215.

Schwartz PJ, Priori SG, Spazzolini C, Moss AJ, Vincent GM, Napolitano C, Denjoy I, Guicheney P, Breithardt G, Keating MT, Towbin JA, Beggs AH, Brink P, Wilde AA, Toivonen L, Zareba W, Robinson JL, Timothy KW, Corfield V, Wattanasirichaigoon D, Corbett C, Haverkamp W, Schulze-Bahr E, Lehmann MH, Schwartz K, Coumel P & Bloise R (2001). Genotype-phenotype correlation in the long-QT syndrome: gene-specific triggers for life-threatening arrhythmias. *Circulation* **103**, 89–95.

Selnick HG, Liverton NJ, Baldwin JJ, Butcher JW, Claremon DA, Elliott JM, Freidinger RM, King SA, Libby BE, McIntyre CJ, Pribush DA, Remy DC, Smith GR, Tebben AJ, Jurkiewicz NK, Lynch JJ, Salata JJ, Sanguinetti MC, Siegl PK, Slaughter DE & Vyas K (1997). Class III antiarrhythmic activity in vivo by selective blockade of the slowly activating cardiac delayed rectifier potassium current I_{Ks} by (*R*)-2-(2,4-Trifluoromethyl)-*N*-[2-oxo-5-phenyl-1-(2,2,2-trifluoroethyl)- 2, 3-dihydro-1*H*-benzo[e][1,4] diazepin-3-yl]acetamide. *J Med Chem* **40**, 3865–3868.

Shah M, Akar FG & Tomaselli GF (2005). Molecular basis of arrhythmias. *Circulation* **112**, 2517–2529.

Shamgar L, Ma L, Schmitt N, Haitin Y, Peretz A, Wiener R, Hirsch J, Pongs O & Attali B (2006). Calmodulin is essential for cardiac I_{Ks} channel gating and assembly: impaired function in long-QT mutations. *Circ Res* **98**, 1055–1063.

Shannon TR, Wang F, Puglisi J, Weber C & Bers DM (2004). A mathematical treatment of integrated Ca dynamics within the ventricular myocyte. *Biophys J* **87**, 3351–3371.

Splawski I, Tristani-Firouzi M, Lehmann MH, Sanguinetti MC & Keating MT (1997). Mutations in the hminK gene cause long QT syndrome and suppress I_{Ks} function. *Nat Genet* **17**, 338–340.

Tohse N (1990). Calcium-sensitive delayed rectifier potassium current in guinea pig ventricular cells. *Am J Physiol Heart Circ Physiol* **258**, H1200–H1207.

Walsh KB & Kass RS (1988). Regulation of a heart potassium channel by protein kinase A and C. *Science* **242**, 67–69.

Wang Q, Curran ME, Splawski I, Burn TC, Millholland JM, VanRaay TJ, Shen J, Timothy KW, Vincent GM, de Jager T, Schwartz PJ, Toubin JA, Moss AJ, Atkinson DL, Landes GM, Connors TD & Keating MT (1996). Positional cloning of a novel potassium channel gene: KVLQT1 mutations cause cardiac arrhythmias. *Nat Genet* **12**, 17–23.

Wang Y, Zankov DP, Jiang M, Zhang M, Henderson SC & Tseng GN (2013). $[Ca^{2+}]_i$ elevation and oxidative stress induce KCNQ1 protein translocation from the cytosol to the cell surface and increase slow delayed rectifier (I_{Ks}) in cardiac myocytes. *J Biol Chem* **288**, 35358–35371.

Weber CR, Piacentino V 3rd, Ginsburg KS, Houser SR & Bers DM (2002). Na^+-Ca^{2+} exchange current and submembrane $[Ca^{2+}]$ during the cardiac action potential. *Circ Res* **90**, 182–189.

Yang T, Kanki H, Zhang W & Roden DM (2009). Probing the mechanisms underlying modulation of quinidine sensitivity to cardiac I_{Ks} block by protein kinase A-mediated I_{Ks} phosphorylation. *Br J Pharmacol* **157**, 952–961.

Yang T, Smith JA, Leake BF, Sanders CR, Meiler J & Roden DM (2013). An allosteric mechanism for drug block of the human cardiac potassium channel KCNQ1. *Mol Pharmacol* **83**, 481–489.

Zeng J, Laurita KR, Rosenbaum DS & Rudy Y (1995). Two components of the delayed rectifier K^+ current in ventricular myocytes of the guinea pig type. Theoretical formulation and their role in repolarization. *Circ Res* **77**, 140–152.

Additional information

Competing interests

No competing interests exist.

Author contributions

Conceived and designed the experiments and simulations: D.C.B, S.M., K.S.G., E.G. and D.M.B. Performed the experiments and simulations: D.C.B, S.M. Analysed and interpreted the results: D.C.B, S.M., K.S.G., E.G. and D.M.B. Wrote the manuscript: D.C.B, S.M., E.G. and D.M.B. All authors approved the final version of the manuscript and all persons designated as authors qualify for authorship, and all those who qualify for authorship are listed.

Funding

This work was supported by the National Institutes of Health NRSA postdoctoral award F32 HL126331 (D.C.B.), R01 grants HL131517 (E.G.) and HL030077 and P01-HL080101 (D.M.B.), the American Heart Association Scientist Development Grant 15SDG24910015 (E.G.) and postdoctoral fellowship 2014POST18380011 (S.M.), and the Heart Rhythm Society post-doctoral fellowship 16OA9HRS (S.M.).